

RSC Advances



This is an *Accepted Manuscript*, which has been through the Royal Society of Chemistry peer review process and has been accepted for publication.

Accepted Manuscripts are published online shortly after acceptance, before technical editing, formatting and proof reading. Using this free service, authors can make their results available to the community, in citable form, before we publish the edited article. This *Accepted Manuscript* will be replaced by the edited, formatted and paginated article as soon as this is available.

You can find more information about *Accepted Manuscripts* in the [Information for Authors](#).

Please note that technical editing may introduce minor changes to the text and/or graphics, which may alter content. The journal's standard [Terms & Conditions](#) and the [Ethical guidelines](#) still apply. In no event shall the Royal Society of Chemistry be held responsible for any errors or omissions in this *Accepted Manuscript* or any consequences arising from the use of any information it contains.

Facile Fabrication of Highly Omniphobic and Self-cleaning Surface Based on Water Mediated Fluorinated Nanosilica Aggregation

Cunqian Wei, Yongqiang Tang, Guangfa Zhang, Qinghua Zhang*, Xiaoli Zhan* and Fengqiu Chen

buhaozhaoReceived 00th January 20xx,
Accepted 00th January 20xx

DOI: 10.1039/x0xx00000x

www.rsc.org/

Liquid repellent surfaces are being promisingly applied in industry and our daily lives. Herein we report a facile and effective sol-gel method for fabricating hybrid coatings with highly omniphobic and self-cleaning properties. The fluorinated hybrid nanocomposite was synthesized via one-step hydrolytic condensation of nanosilica sol, methyltriethoxysilane (MTES) and 3-[(perfluorohexyl sulfonyl) amino] propyltriethoxysilane (HFTES). The solvent mixture of water and 2-propanol surrounding the hydrophobic nanosilica is a key factor in the control of nanoparticle aggregation, which leads to the formation of multi-scale roughness surface with different wettability. The fluorinated nano-sol can be easily coated on various hard and soft substrates by spraying or dipping methods, endowing the substrate with omniphobicity to different organic liquids and biofouling especially solidified egg white. Furthermore, the designed coating shows excellent self-cleaning and anti-adhesion properties in various harsh environments such as high temperature, acid and alkaline treatment and oil contaminate. Owing to the facile method and its remarkable omniphobic abilities, the fluorinated hybrid coatings can be expected to have potential industry applications in a material system requiring robust antifouling, protein resistance and self-cleaning functions.

Introduction

Inspired by the lotus effect, superhydrophobic surfaces with a water contact angle (WCA) higher than 150° and a sliding angle (SA) lower than 10° have received tremendous attention due to their outstanding water repellence and self-cleaning properties^{1, 2}. Water droplets on these superhydrophobic surfaces with combined micro and nanoscale roughness structure can be considered to appear as the Cassie-Baxter state and easy to roll off³⁻⁵. The excellent liquid repellence property is of great importance in commercial and industrial applications, including antisticking, antifouling, anti-icing, self-cleaning, antifogging, marine coating and membrane separation⁶⁻¹⁰. Studies showed that the micro-nano composite roughness structure and low surface energy groups are two crucial factors for the formation of superhydrophobic surfaces¹¹⁻¹⁶. Based on this essential fabrication mechanism, many strategies have been developed to prepare superhydrophobic surfaces^{17, 18}. For instance, Zhan et al. fabricated superhydrophobic materials with the water contact angles of 170.3° by grafting fluorinated polymer chains to nanosilica via surface-initiated activators generated by electron transfer atom transfer radical polymerization⁷. Wang et al. produced a transparent and abrasion-resistant superhydrophobic coating by introduce a PDMS interlayer to support the partially embedded fluoroalkylsilane treated silica nanoparticles¹⁹. Tiemblo et al. have modified silica nanoparticles with oligodimethylsiloxane to form nonfluorinated ultrahydrophobic coatings²⁰. Although these studies are successful in terms of realizing superhydrophobicity, very few of these manufactured surfaces

can be classified as omniphobic that exhibit enhanced repellence to different kinds of liquids such as oils and alcohol.

Stable omniphobic performance is even more challenging to achieve since there is no natural surface that can completely repel organic liquids in the air²¹⁻²³. The key difficulty in fabricating such omniphobic surfaces is to overcome the strong tendency of organic oils with low surface tension to wet surfaces and the adsorption of organic contaminants such as proteins and blood. On the other hand, once the surfaces are placed in oils or applied at high temperature, such as membrane distillation, food packaging and cookware coatings, most of superhydrophobic surfaces will lose part or all of their superhydrophobicity. Ascending temperature often leads to a decline in the surface tension of the contact liquid, which makes the liquid easy to enter the grooves of the micro-nano composite structure on superamphiphobic surfaces²⁴⁻²⁶. In this case, the surface wetting state will generally convert from Cassie-Baxter state to Wenzel state²⁷. So the application of traditional artificial superwetting surfaces is limited.

It is of great significance to fabricate lyophobic even superlyophobic surfaces for both water and organic solvents with low surface energy. Generally, the simultaneous incorporation of topographic features and low surface energy chemistry has been the typical strategy to enhance surface repellency^{21, 28-30}. However, fabrication of omniphobic surfaces is restricted by the control of accurate and tedious surface topography^{23, 31, 32} and complex procedures²² which is too expensive to implement scale and hard to meet the requirements of different applications³³. It has been reported that the fish-scale-like surface showed obvious superoleophobic and self-cleaning properties underwater³⁴⁻³⁷. But this just can be called hydrophilic-oleophobic surface, which will lose its superoleophobicity and convert to oleophilicity in air³⁸. More recently, another strategy for omniphobicity involves lubricant-infused surfaces (SLIPS) based on the structure of the pitcher plant showed superior properties for repelling all types of liquids. SLIPS reveal prominent properties including very low sliding angles and low

^a College of Chemical and Biochemical Engineering, Zhejiang University, Hangzhou 310027, China. E-mail: ghzhang@zju.edu.cn; xlzhan@zju.edu.cn; Fax: +86 571 87991227.

† Electronic Supplementary Information (ESI) available: Additional figures show the XRD results and self-cleaning property, Movie S1 shows superhydrophobicity under oil, and Movie S2-7 shows blood and egg white droplets sliding on FHS-4 treated-glass, filter paper and cotton fabric. See DOI: 10.1039/x0xx00000x

contact angle hysteresis³⁹. However, the main techniques for fabricating SLIPS surfaces, including the construction of surface physical morphology, introduction of compatible groups on the surface and infusing of lubricant, are very complex and difficult to control⁴⁰⁻⁴³. In addition, the surface wetting properties and stability are heavily influenced by the flowability and volatility of the infused lubricant⁴⁴⁻⁴⁷. It is urgently required that new methods for the facile fabrication of uniform omniphobic nanocomposites are developed, as well as a simple strategy to apply it on various substrates on a large scale.

To achieve an ideal material displayed excellent omniphobicity and self-cleaning properties in various environments, herein, one-step sol-gel process was proposed to fabricate novel omniphobic nanocomposite with extraordinary repellence against various organic liquids and biofouling. The hybrid fluorinated surface combining unique micro-nano roughness and ultralow surface energy via hydrolytic condensation of nanosilica sol, methyltriethoxysilane (MTES) and a fluorine contained component (HFTES) was developed. Furthermore, it is a facile approach to precisely regulate the hierarchical structure and wettability of resultant surface via mediating water content. The wettability of the hybrid coatings influenced by morphology has been systematically investigated. The prepared hybrid coating reveals excellent anti-wetting stability under the different temperature environment and ultimate pH values. Besides, this coating also presents good resistance to blood and protein adhesion on various substrates such as metals, glass, fabrics and paper. This work can be expected to provide a new route for the large-scale production of durable omniphobic surfaces.

Experimental

Materials

Nanosilica sol (CR-23-IPA, solid content 30 wt%, 2-propanol dispersion solution, pH=3.6, diameter=106nm, polydispersion=0.06) was purchased from Zhangjiagang Chosen Technology Co., Ltd. 1-Hexanesulfonyl fluoride was provided by Hubei Hengxin Chemical Co., Ltd. 3-[(Perfluorohexylsulfonyl) amino]-propyltriethoxysilane (HFTES) was synthesized according to the literature⁴⁸ and was diluted into 30 wt% with 2-propanol. Methyltriethoxysilane (MTES) was purchased from Aldrich Chemical Co. and was diluted into 30 wt% with 2-propanol. 2-propanol and any other reagents were obtained from Sinopharm Chemical Reagent Co. and used without any further purification.

Preparation of fluorinated hybrid nanocomposite

Nanosilica sol was added in the mixture of MTES and HFTES by magnetic stirring at 30 °C (m [nanosilica sol]: m [MTES]: m [HFTES]=3: 4: 3) to form acidic nano-sol. Then, a certain amount of water was dropwise added into this solution slowly and stirred constantly for 30 min to obtain the hydrophobic fluorinated nano-sol (FNS). After that, obtained fluorinated sol was coated on hard (glass slides and aluminum sheet) or soft

substrate materials (filter paper and cotton fabric) by spraying or dipping methods. The treated soft materials could be bonded to glass slides by double-side tape. All samples were slowly evaporated at ambient temperature for 6h and then thermally treated at 150 °C for 1h.

Surface composition and structure analysis

The particle size in solution was analyzed by Photo Correlation Spectroscopy (PCS) method by Zetasizer 3000HSA (Malvern Ltd., UK). The chemical composition was analyzed by X-ray photoelectron spectroscopy (XPS, Thermo Scientific, USA) with an Al K α X-ray source. The X-ray gun was operated at 14 kV and 350mW, and the analyzer chamber pressure was 10⁻⁹ to 10⁻¹⁰ Pa. The crystallographic structure was characterized on an X-ray powder diffraction system of type Labx XRD-6000 (purchased from Shimadzu, Japan) by monitoring the diffraction angle from 5° to 80°. The surface structures of the hybrid surfaces were observed under a field emission scanning microscopy (FESEM, Hitachi TM-1000) at an accelerating voltage of 20KV. The roughness of the surfaces was analyzed by atomic force microscopy (AFM, Veeco, USA) operated by Multi Mode in tapping mode. The scanning range was 5 μ m \times 5 μ m and the root-mean-square (RMS) roughness value was calculated from the obtained AFM two-dimensional height image.

Surface wettability measurements

Contact angles (CA) for the fluorinated hybrid surfaces were measured from 20 °C to 60 °C through the sessile drop method using a CAM 200 optical contact-angle goniometer (KSV Instruments, Helsinki Finland) and a circulator bath GYY-10. Temperature on the surface was measured by infrared thermometer. The fluorinated surface was heated up to a certain temperature and then liquid droplet was placed on it. The volume of the tested liquid droplet was 5 μ L and measurements were an average based on 10 images of a sample (acquisition rate: 1 image per second). 20 μ L droplets were used for the sliding angle measurements. For the chemical stability of the prepared surfaces, HCl (pH=1) and NaOH (pH=14) solutions were prepared and the samples were immersed into the solutions for 7 days. To prevent vaporization, the containers were well-sealed and kept at room temperature throughout the experiment. The oil-water interfacial tension was determined using pendant drop experiment⁴⁹ at ambient temperature. The hexadecane drop was gradually squeezed out from a hook needle in water environment. When the volume of the oil drop reaches its maximum value, the shape of the drop was captured. The oil-water interfacial tension can be calculated by the shape of the pendant drop. At least five measurements were made at different places on each sample.

Self-cleaning in oil and resistance to blood and protein adhesion tests

The treated and original glass slides were immersed in n-hexadecane and water droplets were dropped onto the oil-contaminated coated surface to test the self-cleaning ability. 50 μ L drops of blood (fresh whole human blood in sodium

heparin was kindly supplied by Zhejiang University Hospital) were deposited on the treated and untreated substrates. The tilting angle was about 20°, and movies and pictures of the rolling process were taken. A droplet of egg white was deposited on the coated Al sheet and then the Al sheet was thermally treated at 150°C for 5 min. After that, the protein was removed and the trace left was observed.

Thermal performance

TGA was carried out on a TGA2050-TA Instrument (USA). The samples were analyzed under the nitrogen atmosphere with heating rate of 10°C/min from room temperature to 850°C.

Results and discussion

Effect of water on surface morphology

Figure 1 illustrates the procedure to prepare the fluorinated hybrid surface (FHS). The FHSs were prepared via a simple sol-gel process by mixing MTES, HFTES and nanosilica gel at the mass ratio of 4:3:3 followed by spraying coating and thermal curing. During this process, with the involvement of mixed

water, the presence of silanol (Si-OH) groups on the nanosilica permits subsequent hydrophobization by the addition of fluorine contained coupling agent HFTES and silane coupling agent MTES and then the fluorinated nano-sol (FNS) was formed. Additionally, the polycondensation of the hydrolyzed MTES and HFTES enhance the adhesive strength of the coated layer. After curing, XRD (see ESI Figure S1†) result shows that four peaks appeared at 2θ values of 5.7°, 17.1°, 23.0° and 28.3°, which could be attributed to the diffraction peaks of SiO₂ reported in the International Center for Diffraction Data (JCPDS data number 31-1233 card), and the broad peak round 20° in the curve of XRD was caused by amorphous silica⁵⁰. It has been recognized that the aggregation of silica or polymer nanoparticles is beneficial for the superhydrophobicity owing to the formation of micro-nano roughness. The water not only hydrolyzes the ethoxy groups of MTES and HFTES, but also improves the permittivity (ε) which is a common measure of the solvent polarity. Different mass of water (ε = 10.2) was added into the solvent of 2-propanol (ε = 4.3) to control the hydrophobic nanoparticles aggregation because of their low colloidal stability in high-polarity solvents.

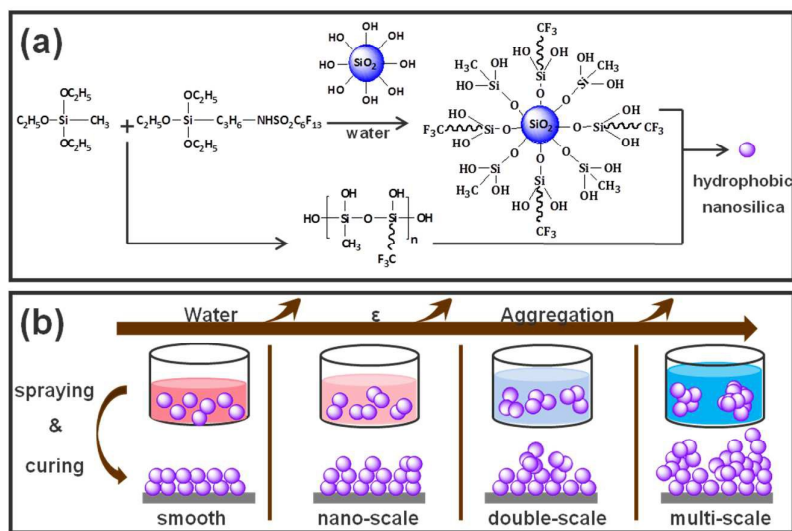


Figure 1. (a) Schematics of the hydrolyzation of MTES, HFTES, the polycondensation between the hydrolyzed MTES, HFTES and nanosilica and (b) then the simplified schematic illustration expected for development of multi-scale roughness from aggregated nanosilicas.

The hydrolysis condensation of MTES, HFTES and nanosilica with addition of water is illustrated in Figure 1a. It is very simple for us to obtain fluorinated hybrid coatings with designed aggregation by control the addition content of mixed water (Figure 1b). The effect of the addition of water content (Table 1) to the fluorinated hydrophobic nanosilica was systematically investigated by Photo Correlation Spectroscopy (PCS) method after diluting to 2wt% by the mixture of 2-propanol and water according to ratio of Table 1. As shown in

Figure 2a, the particle size without any modification is ~ 118nm. With the addition of water, the particle size increased to ~ 755, 2619, 4430nm for FNS-1, 2, 3 respectively, which indicates the aggregation of particles. For FNS-4, the aggregated size largely increased and particles were easy to precipitate. With the addition of more water, agglomeration of the silica nanoparticles would happen and the silica solution became opaque (Figure 2b), which leading to multi-scale roughness structures after curing.

Table 1. Water Contact angle (WCA), contact angle hysteresis (CAH), and sliding angle (SA) of different surfaces achieved by CAM 200 optical contact-angle goniometer at room temperature.

Sample	Hybrid coating	Mass ratio ^a	Diameter (nm)	WCA/°	CAH/°	SA/°
FNS-1	FHS-1	5:2	755	117.3±1.1	12.3±1.3	N/A ^b
FNS-2	FHS-2	5:4	2619	158.1±0.7	4.7±0.8	6.6±1.0
FNS-3	FHS-3	5:6	4430	158.9±1.9	3.4±1.2	3.4±1.9
FNS-4	FHS-4	5:8	9127	157.9±2.0	4.2±0.4	1.7±0.8

^aMass ratio represents the m (acidic nano-sol): m (water). ^bN/A: No angles were recorded. The droplet did not roll off even at a 90° tilting angle.

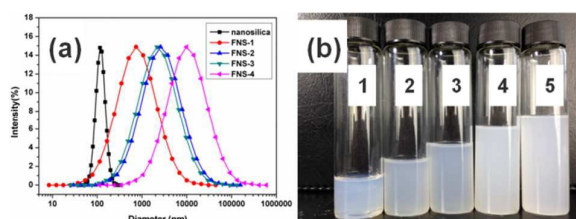


Figure 2. (a) PCS results for nanosilica and fluorinated nano-sol (FNS). (b) Nano particles dispersion with increasing water content. 1- nanosilica, 2- FNS-1, 3- FNS-2, 4- FNS-3, 5- FNS-4.

To better understand the formation procedure of FHS, the effect of water on surface morphology and roughness were investigated by FESEM and AFM. Figure 3 presents the FESEM images of FHS which indicates that various scale roughness is evolved with water addition as described in Table 1. Significant differences between surface morphology under the same magnification could be seen with the same SiO₂ contents. As shown in Figure 3a, MTES and fluorine-contained coupling HFTES were then hydrolyzed and condensed with nanosilicas to get FNS at lower pH environment. And then an organic-inorganic hybrid smooth coating is formed with the RMS of 16.83nm determined by AFM (Figure 4a). With the increase water content, the SiO₂ nanoparticles with the diameter of about 100nm begin aggregate in small amounts and a distinctive wavy surface with nanotexture structure could be obtained (Figure 3b). The RMS roughness of this coating

sample increased to 78.91nm as seen in Figure 4b. When the proportion of water in the solvent continually increased up to 5:6, the permittivity of the blend solvent improves the dispersiveness of nanosilicas reduced quickly. The surface morphology of the hybrid coating sample changed greatly, large amounts of SiO₂ particles aggregate and the protuberances in microscale (~4μm) were observed (Figure 3c). This hybrid coating surface exhibit micro-nano double-scale roughness structure with the RMS of 119.36nm as described in Figure 4c. With further increasing water content to 5:8, as shown in Figure 3d, the multi-scale roughness structure with a protuberances (~9μm) consisting of some aggregated nanoparticles (~1μm) and dispersed nanoparticles (~100nm) was achieved and its RMS roughness increased sharply and reached to 259.40nm (Figure 4d). It was clearly that with different water content, the morphology of the fluorinated hybrid surfaces changed significantly. According to SEM and AFM analysis, it's confirmed that surface roughness of the hybrid coating is dramatically dependent on mediated water content while the content of SiO₂ and other components were unchanged. Accordingly, the change of surface morphology and roughness for the hybrid films could be attributed to the aggregation of nanosilica and the formation of micro-nano composite structure, which was vitally important for its superhydrophobicity and oleophobicity.

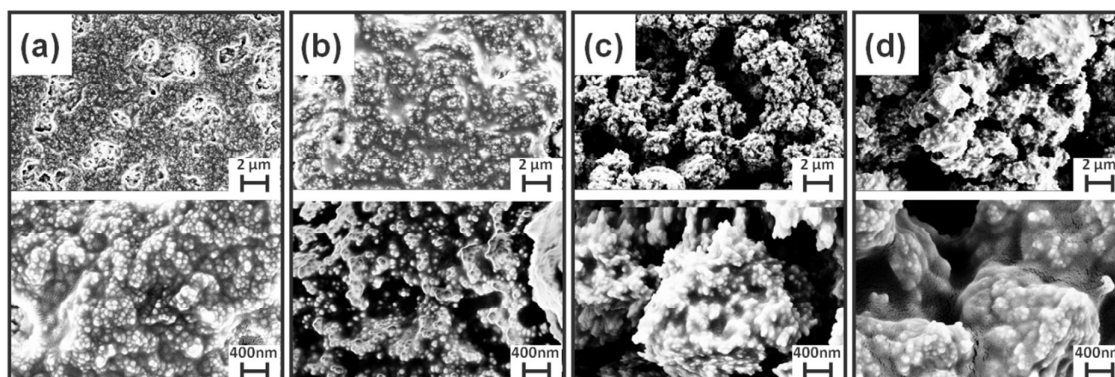


Figure 3. FESEM images of (a) FHS-1, (b) FHS-2, (c) FHS-3, and (d) FHS-4. The next row images are the high-magnification images for (FHS-1~4).

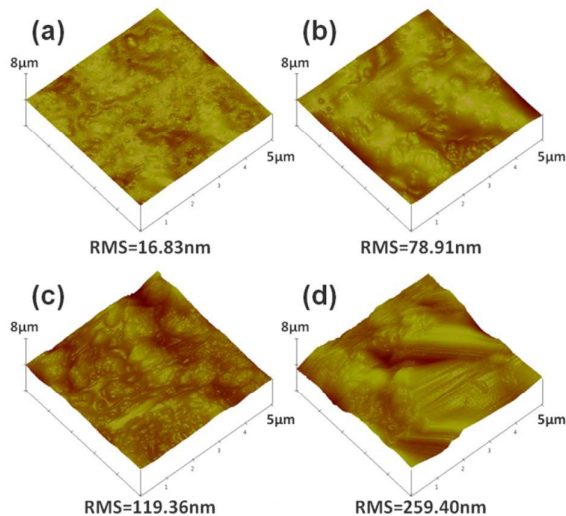


Figure 4. AFM three-dimensional height images of the fluorinated hybrid surfaces. (a) FHS-1, (b) FHS-2, (c) FHS-3, and (d) FHS-4.

Surface wettability

It has been demonstrated that the superwetting properties are governed by surface chemical composition as well as surface morphology²⁸. In this work, the hybrid coating synthesised by sol-gel progress had only different amount of mixed water. After thermal curing, the surface chemical composition of the different coating samples should be the same. The quantitative elemental compositions (Si_{2p} , C_{1s} , O_{1s} and F_{1s}) of the fluorinated hybrid surfaces were evaluated from XPS results. As shown in Figure 5, the high binding energy of 685.5eV attributed to the F element in FHS-3 and 4. There is a higher ratio of F to C in the XPS data (112.46 and 114.35% for FHS-3 and 4 respectively) on the surfaces than that in the bulk (96.28%) due to the significant surface enrichment of the fluorinated chains with low surface energy. This result further demonstrates that the surface chemical composition of the hybrid coatings is similar, even though the surface roughness structure is quite different.

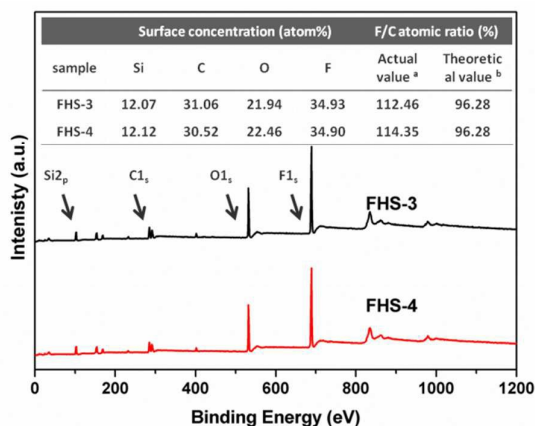


Figure 5. XPS survey spectra of fluorinated hybrid surfaces (FHS). ^a The experimental values based on the XPS measurement. ^b Calculated on the basis of the known composition of the hybrid film.

In addition to surface chemical groups, the multi-scale roughness structure is the key factor affecting the surface wettability. The wetting behavior of the hybrid coating was investigated by the water contact angle (WCA), contact angle hysteresis (CAH), and sliding angle (SA). WCA indicates the hydrophobicity of the surface. CAH and SA directly characterize resistance to mobility. As shown in Table 1, the WCA of the FHS-1 was $117.3^\circ \pm 1.1^\circ$. For the coating sample FHS-2, FHS-3 and FHS-4 with different surface morphologies from nanotexture to multi-scale roughness, the fluorinated hybrid surfaces showed the similar WCAs ($157^\circ \sim 158^\circ$) and CAHs, indicating the strongly enhanced hydrophobicity. But the SA of the three samples decreased with the increasing surface roughness, suggesting that the double and multi-scale hierarchical structures could effectively reduce the sliding resistance and reach an ultralow SA. The water droplets became very unstable on FHS-4, and a gentle vibration could make the water droplets roll away. The superhydrophobic surface with ultralow CAH and SA should endow the hybrid coating with excellent self-cleaning performance (see ESI Figure S2[†]).

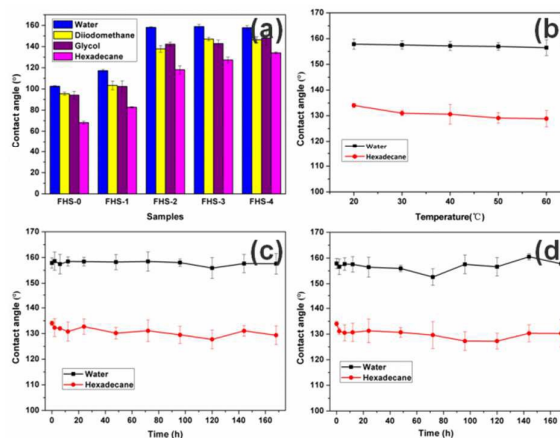


Figure 6. (a) CAs of different samples to various liquids. (b) The CAs on FHS-4 under diverse surface temperatures ranging from 20 to 60°C . The variations of water and oil repellency of FHS-4 after immersion in harsh conditions including pH=1 (c) and pH=14.

At the same time, the fluorinated hybrid surfaces with micro-nano composite structure should exhibit a considerable increase in their organic liquid repellency. Figure 6 shows the static contact angles (CA) of different samples to various liquids under various environments. As illustrated in Figure 5A, water, diiodomethane, glycol and hexadecane droplets with the surface tension of 73.0mNm^{-1} , 50.0mNm^{-1} , 48.0mNm^{-1} and 27.5mNm^{-1} ⁵¹ severally were placed on the FHS and recorded the CAs. A close inspection of the data reveals that FHS-2, FHS-3 and FHS-4 displayed excellent superhydrophobicity but different oleophobicity. The CA values on the FHS-4 surface for the model organic liquids of diiodomethane, glycol and hexadecane were $146.4 \pm 2.0^\circ$, $148.0 \pm 2.8^\circ$ and $134.0 \pm 6.4^\circ$ respectively, which were higher than others. This indicates that the FHS-4 with multi-scale roughness structure possesses more improved oleophobicity or omniphobicity compared

with other samples. These results further confirm that for the low surface energy groups covered surface, only the one with multi-scale roughness structure could achieve excellent omniphobicity toward water and oil droplets with lower surface tension.

For the omniphobic coating with superwetting performance, because of its promising potential in anti-icing application, a lot of researches have been done to study its surface wettability under overcooled temperature. Meanwhile, the omniphobic surface also showed wide application prospect in anti-adhesion or non-stick cookware coatings. But the study of its hydrophobicity and oleophobicity under high temperature was still rare^{24, 26, 27}. In order to explore the thermal stability of the prepared omniphobic surfaces (FHS-4), the static CAs of different liquids on the coatings were tested under a wide temperature range. As shown in Figure 6b, the CAs was slightly decreased with the temperature increasing from ambient temperature (20°C) to 60°C. According to the Etövös rule, the relationship between surface tension and temperature can be described as follows⁵²:

$$\gamma V^{2/3} = k (T_c - T) \quad (1)$$

Where γ is the surface tension, V is the molar volume, k is a constant valid for all liquids. The Etövös constant has a value of $2.1 \times 10^{-7} \text{ J} / (\text{K} \cdot \text{mol}^{2/3})$ and T_c is the critical temperature of liquids where the surface tension is zero at the critical point. The surface tension of contact liquid decreases as its temperature increases, which causes the liquid contact angle decreasing quickly^{24, 27}. So the liquid at high temperature is more prone to spread on the surface. But for water and hexadecane, the static CAs on the coating sample FHS-4 were nearly unchanged with the temperature increasing from 20 to 60°C. This behavior demonstrates that the fluorinated groups covered surfaces with multi-scale roughness possess superior omniphobic performance under higher temperature.

The chemical stability of lyophobic surfaces is a key factor in many applications. The chemical stability of hydrophobicity and oleophobicity for FHS-4 was studied at extreme conditions (pH=1 and 14). At pH=1, as shown in Figure 6c, the CAs of water and hexadecane could keep near 157° and 129° respectively after being immersed for 7 days, while at pH=14, contact angle of water and hexadecane could keep near 157° and 130° separately (Figure 6d). These results indicate that the omniphobic surface remain its superwetting properties relatively well in strong acidic and basic conditions in long term exposure.

The prepared fluorinated nanocomposite sol can be easily sprayed on hard and soft surface and obtained excellent omniphobic and antifouling properties. Figure 7 describes the representative photos of water, glycol, coffee, milk, hexadecane, milky tea, blood, egg white placed on the FHS-4 treated samples and the host substrates. These contaminate liquid droplets can spread on the glass slide quickly and permeate into the filter paper and cotton fabric easily. But on these three surfaces treated by fluorinated nanocomposite sol FHS-4, the droplets of these model liquids all stayed nearly

spherical, presenting a wonderful liquid-repellent property to both soft and hard material surfaces.

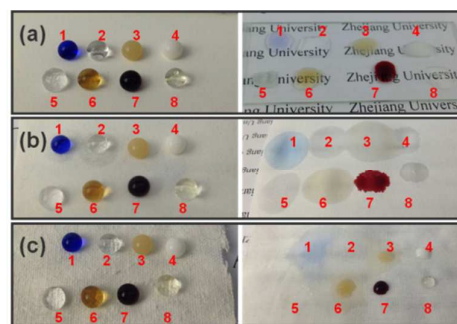


Figure 7. Photos of diverse liquid droplets on FNS-4 treated substrates (left) and host substrates (right). (a) glass slide, (b) filter paper, (c) cotton fabric. Liquid droplets (10µL): 1-water (dyed blue), 2-glycol, 3-milky tea, 4-milk, 5-hexadecane, 6- coffee, 7-blood, 8-egg white.

Self-cleaning property and resistance to protein adhesion

The surface tension of oil is lower than that of water, resulting in the oil easily penetrating through the surfaces, so very few reports have shown any self-cleaning tests in oil because hydrophobic surfaces normally lose their water repellency when even partially contaminated by oil. The prepared omniphobic surface that repels both water and oils provide an effective way to solve this problem. As shown in Figure 8a, water droplet spread and wetted the untreated surfaces when immersed in the oil (hexadecane), but the water droplet still maintain its spherical shape on the FNS-4 treated surface. It has been proposed a criterion that the test liquid droplet floats on the pre-suffused liquid surface when the following condition is satisfied⁴⁹:

$$\Delta\gamma = \gamma_1 \cos\theta_1 - \gamma_2 \cos\theta_2 - \gamma_{12} > 0 \quad (2)$$

where γ_1 and γ_2 are the surface tension of the pre-suffused liquid and the test liquid, θ_1 and θ_2 are their corresponding contact angle on the solid (with air around), γ_{12} is the interfacial tension at the liquid-liquid interface. In this experiment, γ_1 is 27.5 mNm^{-1} for hexadecane, γ_2 is 73.0 mNm^{-1} for water, and γ_{12} is $16.5 \pm 0.4 \text{ mNm}^{-1}$. In the case of glass, $\theta_1 \approx 0^\circ$ and $\theta_2 = 68.5 \pm 0.2^\circ$. According to Equation 2, $\Delta\gamma$ is negative for glass and water droplet would eventually permeate hexadecane and stick to the solid surface. However, for FHS-4, $\theta_1 = 134.0 \pm 6.4^\circ$ and $\theta_2 = 157.9 \pm 2.0^\circ$, thus $\Delta\gamma$ is positive and water droplet would float on the oil and as shown in Figure 8b, water droplets slipped off quickly along the coated glass surface immersed in hexadecane (experimental process are presented graphically in ESI Movie S1†), indicating the surfaces keep their outstanding water repellence in the oil. Figure 8c shows a self-cleaning performance by dust removal test on the prepared omniphobic surface both in air and oil. The omniphobic coating on the glass was partly immersed into oil. The dust was placed deliberately on the surface in air and oil. Water drops were applied to remove the dust on the surface both in air and oil. The dusty surface recovered clean in a short time after dropping a few drops of water, indicating that the fluorinated omniphobic surface keeps the similar

superior water-repellent and self-cleaning properties both in oil and air.

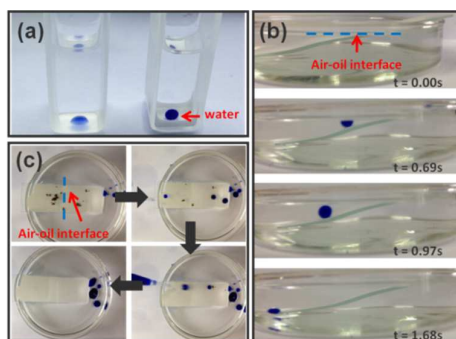


Figure 8. (a) Side view of water droplets placed on blank glass ((a) left) and omniphobic surface FHS-4 ((a) right) that was immersed in oil (n-hexadecane), (b) Water droplet was repelled and easy sliding on the omniphobic surface, (c) Snapshots showing the sand dust removal on the omniphobic surface in the air and oil. Sand dust was put partly in oil and air, the surface was contaminated by oil, water was dropped onto the surface and removed the dust both in air and oil.

The biological protein resistance of the material surface is important for its applications in the area of bioanalysis, cell culture, drug delivery and biomedical engineering. As seen in Figure 7, the viscous liquid containing proteins such as blood and egg white formed high contact angles on the prepared omniphobic surfaces. We further show in ESI Movie S2~4† that blood drop roll off from the FNS-4 treated glass, filter paper and cotton fabric rapidly with no any trace. While, the blood conglutinated on the glass and leave stains on the surfaces (see ESI Figure S3†). The prepared omniphobic surfaces exhibit excellent resistance to the blood adhesion. In order to determine the resistance of the omniphobic coating to the protein adhesion under high temperature, frying egg white on the treated aluminum sheet was performed (Figure 9). At room temperature, the egg white adhered to the untreated aluminum sheet, but it maintained the spherical shape on the treated aluminum and easy to roll off without a trace (see ESI Movie S5~7†). The egg white was then dropped on the treated and untreated aluminum and then be thermally treated for 5min under 150°C. As shown in Figure 9a, the egg white was easily spread on the bare aluminum. After thermal treatment and solidication, egg white gel anchored onto the aluminum surface and was hard to remove. However, the egg white maintained the spherical state before and after thermal treatment on the treated aluminum surface. Furthermore, the egg white gel by thermal treatment was readily removed via a simply method. This behavior demonstrates that the prepared omniphobic surface exhibited distinct resistance to protein both in liquid and solid state.

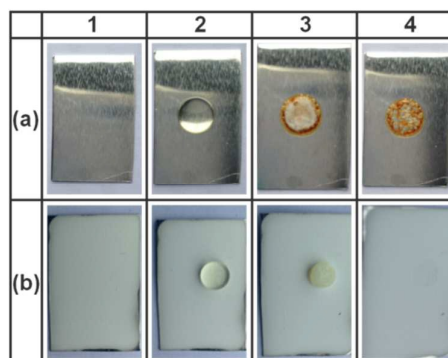


Figure 9. Scheme of protein resistance test in high temperature: (a) Untreated Al (b) FNS-4 treated Al. 1- blank surfaces, 2- a droplet of egg white placed on surfaces at room temperature, 3- protein solidified on surfaces after 5min treatment under 150 °C, 4- surfaces after the removal of protein.

Thermal stability of the omniphobic coatings

The thermal degradation behavior of the fluorinated hybrid coating was evaluated through the TGA measurements. Figure 10 shows the TGA results of FHS-4 coating and nanosilica, and reveals that the hybrid coating degrades in a two-step process. The first degradation (below 3 wt%) of the coatings occurred in the temperature range of 100-350 °C. The small weight loss under this temperature should be attributed to the evaporation of low molecular weight compounds like adsorbed water or solvent that was generated by the condensation of hydroxyl. The second weight loss (about 30 wt%) was observed in the range of 350 °C to 450 °C. This can be attributed to the decomposition of methyl and perfluoroalkyl groups. The test result indicates that the fluorinated sol-gel hybrid coating possess good thermal stability below 350 °C.

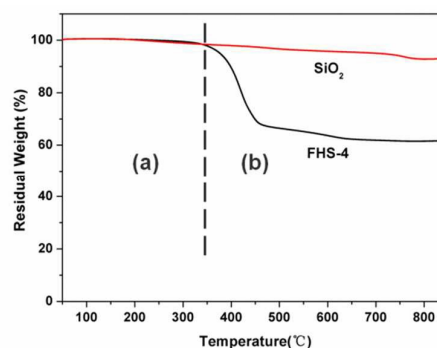


Figure 10. TGA thermograms of nanosilica (SiO_2) and the hybrid coating (FHS-4). (a) Evaporation of residual water and solvent, (b) decomposition and evaporation of methyl and perfluoroalkyl.

Conclusions

We proposed a simple and effective approach to fabricate omniphobic coatings with multi-scale composite structure by hydrolytic condensation of MTES, HFTES and nanosilica sol. Here, different from other complex procedure, the mixed water was used as the main mediating parameter to obtain hierarchic structure. The hybrid nanocomposite could only display multi-scale composite structure and

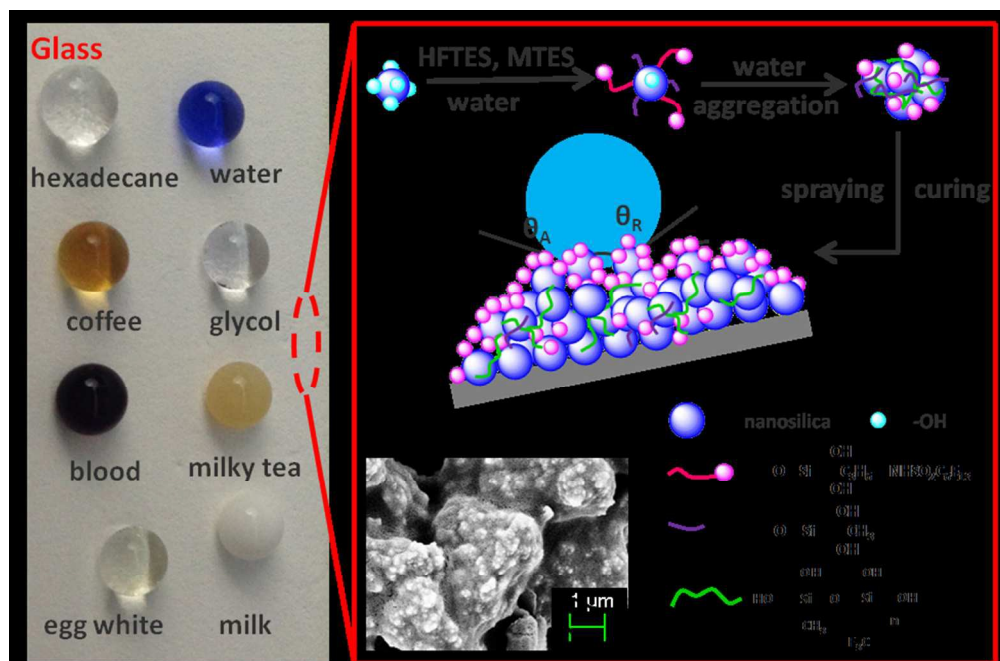
superamphiphobicity when the content of mediated water in the fluorinated nanosilica sol is high enough. The multi-scale roughness structure strengthens the water and oil repellency of the hybrid coatings significantly even under high temperature and keep the similar hydrophobicity and oleophobicity after being treated at extreme acidic (pH=1) and basic (pH=14) conditions for 7 days. Furthermore, the hybrid coating surfaces show outstanding self-cleaning performance since it can maintain superhydrophobicity in oil phase and keep outstanding resistance to blood and protein adhesion and have a great thermal stability below 350 °C. The fluorinated hybrid nanocomposite can be easily used to hard and soft substrates including metals, glass, fabrics and paper. The findings of this study offer a facile, cost-effective method for artificially constructing omniphobic and self-cleaning surfaces with promising commercial application prospect in antifouling, anti-icing, cookware coating etc.

Acknowledgements

The authors would like to gratefully acknowledge the National Natural Science Foundation of China (NSFC) for Award No. 21476195, 21576236 and Zhejiang Provincial Natural Science Foundation of China for Award No.Y14B060038 for supporting this research.

References

- 1 Y. Siand Z. Guo, *Nanoscale*, 2015, **7**, 5922.
- 2 X. Tian, L. Yi, X. Meng, K. Xu, T. Jiang and D. Lai, *Appl. Surf. Sci.*, 2014, **307**, 566.
- 3 D. J. Lee, H. M. Kim, Y. S. Song and J. R. Youn, *ACS Nano*, 2012, **6**, 7656.
- 4 L. Wen, Y. Tian and L. Jiang, *Angew. Chem. Int. Ed.*, 2015, **54**, 3387.
- 5 A. K. Kota, Y. Li, J. M. Mabry and A. Tuteja, *Adv. Mater.*, 2012, **24**, 5838.
- 6 T. Cheng, R. He, Q. Zhang, X. Zhan and F. Chen, *J. Mater. Chem. A*, 2015, **3**, 21637.
- 7 X. Zhan, Y. Yan, Q. Zhang and F. Chen, *J. Mater. Chem. A*, 2014, **2**, 9390.
- 8 M. Wu, B. Ma, T. Pan, S. Chen and J. Sun, *Adv. Funct. Mater.*, 2016, **26**, 569.
- 9 R. Du, X. Gao, Q. Feng, Q. Zhao, P. Li, S. Deng, L. Shi and J. Zhang, *Adv. Mater.*, 2016, **28**, 936.
- 10 Z. Wang, Y. Wang and G. Liu, *Angew. Chem.* 2016, **128**, 1313.
- 11 J. Guo, F. Yang and Z. Guo, *J. Colloid Interface Sci.*, 2016, **466**, 36.
- 12 J. Zhou, J. Fan, Q. Nie and S. Wang, *Nanoscale*, 2016, **8**, 3264.
- 13 N. Wang, D. Xiong, Y. Deng, Y. Shi and K. Wang, *ACS Appl. Mater. Interfaces*, 2015, **7**, 6260.
- 14 D. H. Lee, J. Jeong, S. W. Han and D. P. Kang, *J. Mater. Chem. A*, 2014, **2**, 17165.
- 15 Y. Zhou, J. Li, Q. Zhang and Z. Luo, *AIChE J.*, 2014, **60**, 4211.
- 16 Y. Zhou, J. Li, Q. Zhang and Z. Luo, *Langmuir*, 2014, **30**, 12236.
- 17 G. Cavallaro, D. I. Donato, G. Lazzara and S. Milioto, *J. Phys. Chem. C*, 2011, **115**, 20491.
- 18 G. Cavallaro, G. Lazzara, S. Milioto and F. Parisi, *Langmuir*, 2015, **31**, 7472.
- 19 P. Wang, M. Chen, H. Han, X. Fan, Q. Liu and J. Wang, *J. Mater. Chem. A*, 2016.
- 20 R. de Francisco, P. Tiemblo, M. Hoyos, C. González-Arellano, N. García, L. Berglund and A. Synytska, *ACS Appl. Mater. Interfaces*, 2014, **6**, 18998.
- 21 L. Wang and T. J. McCarthy, *Angew. Chem. Int. Ed.*, 2016, **55**, 244.
- 22 T. P. Nhung Nguyen, P. Brunet, Y. Coffinier and R. Boukherroub, *Langmuir*, 2010, **26**, 18369.
- 23 A. Tuteja, W. Choi, J. M. Mabry, G. H. McKinley and R. E. Cohen, *Proc. Natl. Acad. Sci. U. S. A.*, 2008, **105**, 18200.
- 24 Y. Liu, X. Chen and J. H. Xin, *J. Mater. Chem.*, 2009, **19**, 5602.
- 25 S. Peng, D. Tian, X. Yang and W. Deng, *ACS Appl. Mater. Interfaces*, 2014, **6**, 4831.
- 26 F. Wan, D. Yang and E. Sacher, *J. Mater. Chem. A*, 2015, **3**, 16953.
- 27 Z. Yu, J. Yang, F. Wan, Q. Ge, L. Yang, Z. Ding, D. Yang, E. Sacher and T. T. Isimjan, *J. Mater. Chem. A*, 2014, **2**, 10639.
- 28 P. Zhang, S. Wang, S. Wang and L. Jiang, *Small*, 2015, **11**, 1939.
- 29 J. Long, L. Pan, P. Fan, D. Gong, D. Jiang, H. Zhang, L. Li and M. Zhong, *Langmuir*, 2016, **32**, 1065.
- 30 Y. Lu, S. Sathasivam, J. Song, C. R. Crick, C. J. Carmalt and I. P. Parkin, *Science*, 2015, **347**, 1132.
- 31 R. Dufour, M. Harnois, V. Thomy, R. Boukherroub and V. Senez, *Soft Matter*, 2011, **7**, 9380.
- 32 K. Rykaczewski, A. T. Paxson, M. Staymates, M. L. Walker, X. Sun, S. Anand, S. Srinivasan, G. H. McKinley, J. Chinn, J. H. J. Scott and K. K. Varanasi, *Sci. Rep.*, 2014, **4**.
- 33 N. K. Neelakantan, P. B. Weisensee, J. W. Overcash, E. J. Torrealba, W. P. King and K. S. Suslick, *RSC Adv.*, 2015, **5**, 69243.
- 34 A. Venault, H. Yang, Y. Chiang, B. Lee, R. Ruaan and Y. Chang, *ACS Appl. Mater. Interfaces*, 2014, **6**, 3201.
- 35 M. Sin, W. Lin, J. C. Chen, A. Higuchi, J. Zheng, A. Chinnathambi, S. A. Alharbi and Y. Chang, *Int. J. Polymer. Mater.*, 2016, **65**, 409.
- 36 H. S. Sundaram, X. Han, A. K. Nowinski, J. Ella-Menye, C. Wimbish, P. Marek, K. Senecal and S. Jiang, *ACS Appl. Mater. Interfaces*, 2014, **6**, 6664.
- 37 H. S. Sundaram, X. Han, A. K. Nowinski, N. D. Brault, Y. Li, J. Ella-Menye, K. A. Amoaka, K. E. Cook, P. Marek, K. Senecal and S. Jiang, *ACS Appl. Mater. Interfaces*, 2014, **6**, 6664.
- 38 K. Chen, S. Zhou and L. Wu, *ACS Nano*, 2016, **10**, 1386.
- 39 T. Wong, S. H. Kang, S. K. Y. Tang, E. J. Smythe, B. D. Hatton, A. Grinthal and J. Aizenberg, *Nature*, 2011, **477**, 443.
- 40 I. Okada and S. Shiratori, *ACS Appl. Mater. Interfaces*, 2014, **6**, 1502.
- 41 K. Manabe, S. Nishizawa, K. Kyung and S. Shiratori, *ACS Appl. Mater. Interfaces*, 2014, **6**, 13985.
- 42 S. Anand, A. T. Paxson, R. Dhiman, J. D. Smith and K. K. Varanasi, *ACS Nano*, 2012, **6**, 10122.
- 43 U. Manna and D. M. Lynn, *Adv. Mater.*, 2015, **27**, 3007.
- 44 Y. Ding, J. Zhang, X. Zhang, Y. Zhou, S. Wang, H. Liu and L. Jiang, *Adv. Mater. Interfaces*, 2015, **2**, 1500177.
- 45 C. Howell, T. L. Vu, C. P. Johnson, X. Hou, O. Ahanotu, J. Alvarenga, D. C. Leslie, O. Uzun, A. Waterhouse, P. Kim, M. Super, M. Aizenberg, D. E. Ingber and J. Aizenberg, *Chem. Mater.*, 2015, **27**, 1792.
- 46 J. Zhang, A. Wang and S. Seeger, *Adv. Funct. Mater.*, 2014, **24**, 1074.
- 47 J. Zhang, L. Wu, B. Li, L. Li, S. Seeger and A. Wang, *Langmuir*, 2014, **30**, 14292.
- 48 Y. Tang, Q. Zhang, X. Zhan and F. Chen, *Soft Matter*, 2015, **11**, 4540.
- 49 H. Liu, P. Zhang, M. Liu, S. Wang and L. Jiang, *Adv. Mater.*, 2013, **25**, 4477.
- 50 F. Kotz, K. Plewa, W. Bauer, N. Schneider, N. Keller, T. Nargang, D. Helmer, K. Sachsenheimer, M. Schäfer, M. Worgull, C. Greiner, C. Richter and B. E. Rapp, *Adv. Mater.*, 2016, **28**, 4646.
- 51 S. Peng, X. Yang, D. Tian and W. Deng, *ACS Appl. Mater. Interfaces*, 2014, **6**, 15188.
- 52 R. Etövös, *Ann. Phys.*, 1886, **263**, 448.



165x108mm (150 x 150 DPI)